

Novel technique for supernova detection with IceCube

L. Demirörs, M. Ribordy and M. Salathe

High Energy Physics Laboratory, EPFL, CH-1015 Lausanne, Switzerland

The current supernova detection technique used in IceCube relies on the sudden deviation of the summed photomultiplier noise rate from its nominal value during the neutrino burst, making IceCube a ≈ 3 Megaton effective detection volume - class supernova detector. While galactic supernovae can be resolved with this technique, the supernova neutrino emission spectrum remains unconstrained and thus presents a limited potential for the topics related to supernova core collapse models.

The paper elaborates analytically on the capabilities of IceCube to detect supernovae through the analysis of hits in the detector correlated in space and time. These arise from supernova neutrinos interacting in the instrumented detector volume along single strings. Although the effective detection volume for such coincidental hits is much smaller ($\gtrsim 35$ kton, about the scale of SuperK), a wealth of information is obtained due to the comparatively low coincidental noise rate. We demonstrate that a neutrino flux from a core collapse supernova will produce a signature enabling the resolution of rough spectral features and, in the case of a strong signal, providing indication on its location.

We further discuss the enhanced potential of a rather modest detector extension, a denser array in the center of IceCube, within our one dimensional analytic calculation framework. Such an extension would enable the exploration of the neutrino sky above a few GeV and the detection of supernovae up to a few 100's of kilo parsec. However, a 3 – 4 Mpc detection distance, necessary for routine supernova detection, demands a significant increase of the effective detection volume and can be obtained only with a more ambitious instrument, particularly the boosting of sensor parameters such as the quantum efficiency and light collection area.

I. INTRODUCTION

Much of the underlying physics of a core collapse supernova remains unexplored, the mechanism leading to the explosion not well understood. Though it is clear that neutrinos play a major role in the dynamics of the explosion, carrying away 99% of the energy emitted by the dying star. The observation of neutrinos in the provenance of SN 1987A in several experiments [1–3] has confirmed the crucial role they play in the overall picture. The limited number of detected neutrinos, however, has not provided enough statistics to constrain current supernova models. This may only be achieved with a detector performing routine SN detection, about one per year.

The idea of using IceCube as a supernova detector was first discussed in [4, 5]. The method is based on the sudden increase in the photomultiplier count rate on a timescale of the order of 10 seconds: qualitatively, the release by a supernova at $d = 10$ kpc with a total amount of energy of 10^{58} MeV in neutrinos of about 20 MeV corresponds to a flux of $7 \cdot 10^{14} \text{ m}^{-2}$. In its completed configuration and with its data acquisition system, IceCube has about 3 Mton effective detection volume and a reach of about 50 kpc at 5σ C.L. detection level. Here, we extend that method and assess the potential of IceCube and several prospective detector configurations by considering multiple hit detection in a single or neighboring sensors from individual neutrino interactions. We demonstrate that multi-hit modes enable the extraction of new observables related to the features of the neutrino emission spectrum and the supernova location, not accessible by means of the original method. This new data stream could help study questions related to supernova dynamics (neutronization burst, accretion and cooling phase,

see [7] and references therein) or fundamental questions of particle physics, related to the nature of the neutrino [8, 9]. The observation of electron neutrinos from the early neutronization burst could disentangle the neutrino hierarchy [11], provided a sufficiently large mixing angle θ_{13} as indicated recently [10].

These new detection modes are conceptually situated between a full reconstruction of the events and the current search method balancing the simplicity of the latter with the richness in information of the former. We show that the loss of information in the current method is not necessary and that a very elementary reconstruction, implemented through the coincident hit methodology, can enhance the information obtained during a supernova explosion. In fact, it would appear natural to extend the new detection modes to a full reconstruction of supernova events in the case of a very densely instrumented volume.

According to [12, 13], the estimated SN rate from our galaxy is about 0.03/yr. It increases to 0.1/yr within 1 Mpc and about 1/yr within 4 Mpc. We will see that extending the reach of a future detector to such a large distance is quite challenging given the quick decrease of the interaction density with distance. SuperK, with its 32 kton fiducial volume, remains at the moment an instrument of choice [14]. IceCube [15] with its 86 strings and this new detection methodology could become a serious competitor, even surpass it, provided a deep and denser core extension installation. There are several good reasons for such an extension beyond an enhanced potential for SN detection, mainly the detection of individual high energy neutrinos down to several GeV related to multiple physics aspects, such as neutrino sources in the Southern sky [16, 17], indirect detection of dark matter

down to lower mass [18–20] and neutrino particle physics [21].

This contrasts with the potential of other projected 100 kton-class detectors, e.g. liquid scintillator LENA [22] or liquid Argon detectors [23], which will have an extended potential for SN detection but comparatively small fiducial volumes at energies beyond GeV. Especially the latter are complementary to water or ice-based Cherenkov detectors, since they are more sensitive to the electron neutrino channel, providing a better access to the physics during the neutronization burst [24]. Combining the measurements from these detectors, which differ not only in their sensitive material, but in their geographic location, would enable the study of matter effects and neutrino hierarchy by observing neutrinos from the same supernova from different viewpoints with a high detection probability.

Finally, a large detector will not only increase the distance reach for SN but also provide large event statistics for galactic SN with possible resolution for their location, leading through a SN alert system (SNEWS [25]) to the optical detection of obscured and otherwise missed galactic SNe.

In Section 2, we define the studied configuration and the benchmark supernova neutrino flux. We present the effective volume analytical calculations in Section 3 and their consequences in Section 4.

II. DEFINITIONS AND METHODOLOGY

A. Detectors and sensors

Configurations

In the following, we consider several detector configurations [26]:

a. The baseline IceCube configuration (IC), with a number of sensors $N_{\text{OM}} = 4800$, arranged $L = 17$ m apart along 80 strings.

b. The Deep Core configuration (DC), with $N_{\text{OM}} = 320$, $L = 7$ m apart on 8 strings.

c. The Dense and Deep Core configuration: An imaginative futuristic low energy extension in alternative configurations denoted DDC, $\text{DDC}_{4\pi}$, $\text{DDC}_{4\pi}^{\text{VL}}$ composed of 24 strings with 150 sensors each, $N_{\text{OM}} = 3600$, and with a spacing between modules of $L = 3$ m. In configurations with 4π subscript, the sensitive area of the spherical module has a 4π acceptance, for instance the modules designed for KM3NET [27]. The $\text{DDC}_{4\pi}^{\text{VL}}$ configuration has also a larger sensitive area and higher Q.E. In addition, we assess the potential of the full acceptance configurations with extremely low noise modules (100 Hz).

A short local coincidence is the occurrence of two or more hits within specific time windows δt 's in a single sensor or in two neighboring sensors, also referred to as

optical modules. The systematic recording of these coincidences would require the implementation of a dedicated data acquisition mode and its corresponding data stream. We study in this paper several detection modes ij , $i \leq 2$ and $j \leq 1$, referring to the coincidental detection of i hits with a module and j hits with the module just above along a sensor string.

In this paper we do not consider coincident hits between strings, so string spacing is not a parameter in this study. We refer therefore to our study as 1D analytic approximation. We also restrict the study to nearest neighbor (NN) coincidences.

Sensor geometry

The geometry of the optical modules for the three detector configurations IC, DC and DDC is illustrated in Fig. 1. The modules [28] are composed of a 0.5 inch enveloping glass sphere (to withstand the pressures at the large deployment depths, in particular during the ice refreezing process) with an external radius $R \equiv R_{\text{OM}} = 13$ inch, enclosing a photomultiplier R7081-02 made by Hamamatsu Photonics [33]. The glass and contact gel between the PMT and the glass introduce a 350 nm lower cutoff.

In all configurations except $\text{DDC}_{4\pi}$, the photocathode sensitive surface of the sensor covers a fraction of the sphere slightly smaller than the half sphere. The resulting cutoff angle on the sensitive surface is given by $\theta_{\text{max}} - \pi/2$, where θ_{max} is the limit on the incoming direction of Cherenkov photons at which they can intersect the sensitive surface of the module. Given the specifications of the IceCube photomultiplier, we can estimate $\pi - \theta_{\text{max}} \approx 25^\circ$.

Viewed under an angle θ , the projected area of the sensitive surface is

$$A \equiv A_{\text{OM}}(\theta) = \pi R R(\theta), \quad (1)$$

where

$$R(\theta) = R \frac{1 - \cos(\theta_{\text{max}} - \theta)}{1 - \cos \theta_{\text{max}}} H(\theta_{\text{max}} - \theta) \quad (2)$$

for a module sphere looking down and with a photocathode sensitive area cutoff angle $\theta_{\text{max}} - \pi/2$, as illustrated on Fig. 1.

Sensor photon detection efficiency

The photon detection efficiency (PDE) of the sensitive surface $\chi(\lambda)$ has been measured somewhere [50], it combines the PMT Q.E., the transparency of the surrounding glass and the contact gel which couples the glass to the PMT. Averaged over a λ^{-2} Cherenkov spectrum between 300 and 650 nm, and accounting for an amplitude trigger threshold keeping $\epsilon_{\text{thr}} = 90\%$ of the p.e.'s, it yields an integrated PDE

$$\langle \chi \rangle = \frac{\epsilon_{\text{thr}}}{\int d\lambda/\lambda^2} \int \chi(\lambda)/\lambda^2 d\lambda = 7.3\% \quad (3)$$

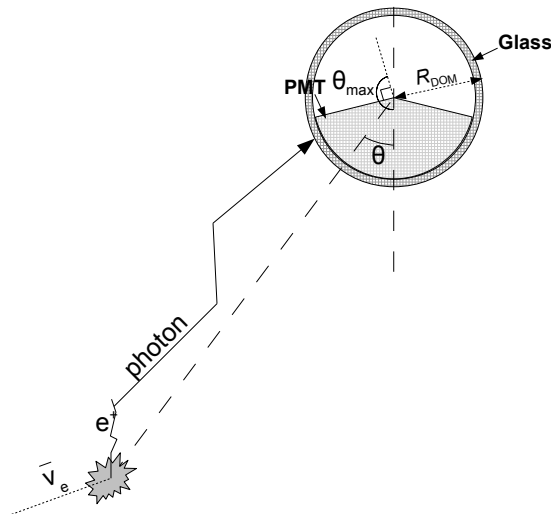


FIG. 1: Illustration of the sensor geometry and definition of θ and θ_{\max} .

for the regular IC sensors. The high quantum efficiency sensors deployed in DC are assumed to have a PDE 30% higher [26]. The same assumption is made for the DDC and DDC $_{4\pi}$ configurations. In contrast to previous works [5], $\langle\chi\rangle$ is significantly lower, due to a regular optical module peak PDE of about 14% at 420 nm.

Although $\langle\chi\rangle$ is a fair approximation for our analytical estimates presented in the next section, a toy Monte Carlo simulation should implement the complete wavelength dependence of $\chi(\lambda)$ given that the propagation of photons in the ice medium is described in terms of wavelength-dependent scattering and absorption lengths λ_{scatt} and λ_{abs} [34]. This dependence in the propagation cannot be disentangled from that of the PDE.

Sources of background noise

The following types of background may limit the applicability of the coincident hit detection methodology:

a. Cosmic-ray induced muons. A fraction will travel down to the detector and produce coincident hits. We assume that most of these events are muons dying in the upper layers of the detector: they barely enter the fiducial volume and produce light on a very limited number of external sensors. We assume that this event class can be adequately rejected. Some higher energy muons however penetrate deeper into the detector and although most of them can be vetoed given their specific topology, some may leave a signature well inside the instrumented volume mimicking the coincidence signature under investigation. We would expect the resulting rate to be minimal and thus neglect it, but this specific topology should still be further studied separately by means of the experimental data, to properly substantiate this statement.

b. Low E atmospheric neutrino-induced muons or electronic showers. This background is constituted by low energy neutrinos in the 10 MeV – 1 GeV range [35–

37]. The interaction rate is very limited, well below 1 Hz, in a Gton ice volume.

c. Sensor correlated noises at μs and ms time scales, due respectively to photomultiplier afterpulse and radioactive decay chains [45]. The afterpulse components of the dark noise come with well defined [28, 46] delays after the original photo-induced signal, larger than the time windows used below for coincidental hit detection within a single sensor, so that (1) it does not pollute and therefore impede the coincidental hit detection method for this specific channel, (2) it can be filtered out by means of an offline analysis, leading to an effective noise rate significantly smaller than measured (dark count reduced from 580 Hz to $r \equiv r^{10} = 440$ Hz [28, 29]). This reduced dark count rate value is thus considered to calculate the probability of the noise. Note that the deadtime introduced by this afterpulse filter is negligible ($\lesssim 0.5\%$).

The effect of ms timescales of correlated noise is more complex and it is not clear whether it would affect the potential of the new methodology when applied to specific channels with multiple hits in a single sensor.

We define the hit times $\{t_i\}_i$, a hit time window by its width $(\delta t)_{ij}$ and an arbitrary time shift t_{ij} . Hits i and j belong to the time window if $|(t_j - t_i) - t_{ij}| < (\delta t)_{ij}/2$. We restrict the study to several qualitatively complementary NN detection modes,

- single sensor hit: mode 10 or "1+0";
- two photons detected in the same sensor: mode 20 or "2+0";
- a single hit detected in two NN sensor: mode 11 or "1+1";
- three photons detected at times t_1, t_2 (in the same sensor, $t_1 < t_2$) and t_3 (in the sensor above): mode 21 or "2+1".

The noise rates of two hit coincidences r^{20} and r^{11} given by

$$r^{11} = r^2 (\delta t)_{13} \text{ and } r^{20} = 2r^2 (\delta t)_{12} \quad (4)$$

(the latter factor two because hits at a single module are indistinguishable). The coincidental noise rate with two hits in the lower sensor and a single hit in its upper neighbor is

$$r^{21} = 2r^3 (\delta t)_{12} (\delta t)_{13}. \quad (5)$$

Note that in the IceCube detector, only the lower hemisphere of the optical module is sensitive and therefore, a hit in the upper sensor coming after a hit in the lower sensor is strongly preferred (i.e. an optimal time window will have $t_{13} > 0$). This is not true for some of the futuristic detector configurations which have a uniform sensitive surface: in this case, we will choose $t_{13} = 0$.

The detector coincidental noise rate scales linearly with the number of sensors (the number of independent pairs

is almost equivalent to the number of sensors, provided that the number of sensor along a string is $\gg 1$).

IceCube has a system that records local coincidences within a $2\ \mu\text{s}$ ($\pm 1\ \mu\text{s}$) time window up to the next-to-nearest neighbor (there are four such neighbors) [30]. The rate of such coincidences, called *hard local coincidences* (HLC), should be therefore of the order of $r_{1\ \mu\text{s}}^{\text{HLC}} = 4 \times 2 \times r_{1\ \mu\text{s}} \approx 1.55\ \text{Hz}$ per optical module. For our purpose, we consider the rate of coincidental events within a much shorter coincidence time window with $\Delta t = 30 - 150\ \text{ns}$ involving one neighboring sensor corresponding to a coincidental noise rate of $r_{30-150\ \text{ns}} \approx 0.006 - 0.03\ \text{Hz}$ per sensor.

A SN signal becomes significant when the number of coincidental events integrated over the typical duration of the SN neutrino emission (about 3 seconds) takes values larger than the fluctuations of the noise rate r^{ij} , corresponding to the various event classes.

B. Supernova neutrino emission models

We have chosen to study several flux models of rather modest luminosity. Our main benchmark flux model is the "SF" model (also referred to as "Garching" model), an 8.8 solar mass electron capture supernova, discussed in [6] and which may represent a large fraction of all supernovae.

Furthermore, in this paper we will only consider the predicted anti-electron neutrino flux, focusing solely on the inverse beta decay (IBD) reaction in ice, *i.e.* $\bar{\nu}_e + \text{p} \rightarrow \text{n} + \text{e}^+$. For one, in water or ice, which are natural media for high energy neutrino telescopes, the (anti-)electron neutrino interaction with oxygen has a much higher energy threshold and a quite significantly smaller CC cross section at the energies of interest [31]. This largely makes this channel subdominant for the interaction rate in the detector compared to the IBD reaction yield. Moreover, a large fraction of the neutrino energy is absorbed into binding energy, reducing the Cherenkov light yield and dramatically suppressing the potential of this reaction channel given that our methodology relies on the coincident detection of Cherenkov photons in neighboring sensors. We also neglect the elastic interaction channel $\bar{\nu}_e + \text{e}^- \rightarrow \bar{\nu}_e + \text{e}^-$ which has an even lower cross section than the oxygen channel [32].

The anti-electron neutrino flux luminosity is given by

$$\frac{d\tilde{\Phi}_{\bar{\nu}_e}}{dE_{\nu}}(E_{\nu}, d) = \frac{1}{4\pi d^2} \int_0^{\tilde{t}} \frac{L(t)}{\langle E_{\nu} \rangle(t)} f_{\alpha(t), \langle E_{\nu} \rangle(t)} dt \quad (6)$$

where

$$f_{\alpha, \langle E_{\nu} \rangle}(E_{\nu}) = \frac{(1 + \alpha)^{1+\alpha}}{\langle E_{\nu} \rangle \Gamma(1 + \alpha)} \left(\frac{E_{\nu}}{\langle E_{\nu} \rangle} \right)^{\alpha} e^{-(1+\alpha) \frac{E_{\nu}}{\langle E_{\nu} \rangle}} \quad (7)$$

and with the time-dependent model parameters luminosity $L(t)$, average neutrino energy $\langle E_{\nu} \rangle(t)$ and pinch parameter $\alpha(t)$. Their time evolution can be found in [6]. It

is interesting to note, as illustrated in Fig. 2, that the parameters α and $\langle E \rangle$ can be very well fitted with Eq. 7 in order to match the integrated neutrino flux and positron density up to a certain time.

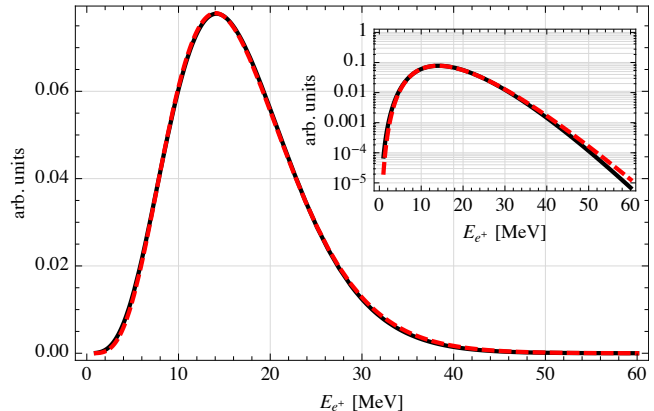


FIG. 2: Positron spectrum, integrated up to \tilde{t} . Dashed line is the result of fitting $\alpha = 4.77$ and $\langle E_e \rangle = 16.97\ \text{MeV}$.

The neutrino flux integration time \tilde{t} , which closely optimizes the potential in terms of distance reach of the coincident hit method is derived by maximizing the signal to the square root of noise ratio, assuming an exponential luminosity decrease, in good qualitative agreement $\forall t \gtrsim 1\ \text{s}$, with $t_0 \approx 2.35\ \text{s}$, of the luminosity evolution in the Garching model (a usual luminosity decrease in $(1 + t/t_0)^{-\beta}$ does not fit well).

The argument could be more sophisticated, e.g. by using a refined likelihood temporal analysis.

The integrated signal (the supernova neutrinos producing an event) up to time \tilde{t} is $S(\tilde{t}) = \int_0^{\tilde{t}} s_0 e^{-t/t_0} dt = s_0 t_0 (1 - e^{-\tilde{t}/t_0})$. The detector noise is assumed gaussian with count fluctuation of a complete detector configuration $\sqrt{\tilde{\mu}} = \sqrt{N_{\text{OM}} r \tilde{t}}$ within an integration time \tilde{t} , where r is the noise rate of a specific mode. \tilde{t} is determined

$$\frac{d}{d\tilde{t}} \frac{S(\tilde{t})}{\sqrt{\tilde{\mu}}} = 0 \quad (8)$$

leading to

$$\tilde{t} = \frac{t_0}{2} (e^{\tilde{t}/t_0} - 1). \quad (9)$$

We extract $\tilde{t} = 2.95\ \text{s}$ for $t_0 = 2.35\ \text{s}$ and we note that \tilde{t} is independent of s_0 (proportional to the luminosity), of the noise rate r and of the significance of the observation.

The luminosity at early times is larger than in this description, so that this integration time \tilde{t} constitutes a conservative upper bound regarding the potential of the method: if more precisely assessed, \tilde{t} and thus the integrated noise would be reduced.

The integrated anti-electron neutrino luminosity within this time-span \tilde{t} is $\tilde{L} = 2.13 \cdot 10^{52}$ erg, and the flux $\tilde{\Phi}_{\bar{\nu}_e} = 0.89 \cdot 10^{15} \text{ m}^{-2}$. The average neutrino energy is $\langle \tilde{E}_{\bar{\nu}_e} \rangle = 12.5 \text{ MeV}$. \tilde{L} is about three quarter of the total luminosity. It is important to note, when comparing the limiting distance up to which a SN can be discovered, that the total luminosity is about 56% of the one considered in [13].

We have also calculated the outcome of the novel detection methodology for neutrino spectra which obey a Fermi-Dirac distribution,

$$f_{\eta,T}(E_\nu) = N(\eta, T) \frac{(E_\nu/T)^2}{1 + e^{E_\nu/T - \eta}} \quad (10)$$

where $N(\eta, T) = -(2TLi_3(-e^\eta))^{-1}$. We have normalized the amount of energy released over \tilde{t} to be equal to the Sf model, for two temperature, $T = 5 \text{ MeV}$ and $T = 6.5 \text{ MeV}$. Although the average neutrino energies, $\langle E_{\bar{\nu}_e} \rangle_{T=5 \text{ MeV}} = 15.8 \text{ MeV}$ and $\langle E_{\bar{\nu}_e} \rangle_{T=6.5 \text{ MeV}} = 20.5 \text{ MeV}$, are larger resulting in smaller flux than in the Sf model, the interaction density is increased by more than 50% due the IBD cross section increase turning into a considerable increase in the coincidental hit rate (by a factor > 2) as will be seen.

C. Discovery potential and sensitivity

We assess the discovery and learning potential by requesting the signal over square root of noise ratio $s = 5$ and $s = 1$ for the C.L. in σ unit, respectively, using the Poissonian distribution p_μ : given a mean number of expected coincidental noise events $\tilde{\mu}$, a minimum number of $\geq m$ events is required to reach significance $\geq s$,

$$\min_m \left\{ m \mid p_{\tilde{\mu}}(0) + \sum_{k=1}^m p_{\tilde{\mu}}(k) \geq \text{erf}\left(\frac{s}{\sqrt{2}}\right) \right\}. \quad (11)$$

The distance reach is therefore given by

$$d_{10 \text{ kpc}}^s = \sqrt{n_s / (m - \tilde{\mu})}, \quad (12)$$

where $d_{10 \text{ kpc}}^s$ is the distance in 10 kpc units and n_s is the number of signal events from a SN explosion at 10 kpc.

An advantage of the detection method relying on coincidental hits arises from a more gaussian distributed coincidental noise rate (while the single hit noise rate distribution has non gaussian tails, requesting coincidences dilutes them). The false alarm rate (assuming gaussianity) for $s = 5$ is roughly $\tilde{t}/\text{erfc}(5/\sqrt{2})/2 = 3 \text{ yr}^{-1}$.

$s = 1$ is a requirement too weak and not adequate for IceCube to trigger as a standalone detector, but where IceCube may help establishing stronger constraints by enhancing the quality of an observation: it sets the distance scale for IceCube to contribute in supplementing information to observations made by other instruments detecting e.g. a neutrino or an optical signal. In the latter case, of course, IceCube would have to buffer the relevant information because of the few hours delay between the neutrino and the optical signal.

III. ESTIMATE OF SINGLE AND COINCIDENT HIT DETECTION RATE

The positron effective detection volume as a function of the neutrino energy is the product of the number of target protons in the interaction volume and of the fraction of uniformly distributed positrons leading to a detection. It is an important and well defined concept for our analysis because the positron tracks are nearly point-like with a path length of about 10 cm in average, a small distance compared to the mean distance between a positron and a sensor in which it leaves a signature. This enables the estimation of the response of the detector to a given flux of low energy neutrinos.

The positron effective volume for coincidence of order k at a single module is denoted $V_{\text{eff}}^k(E)$, where $k = 1, 2$ for the detection of a single hit resp. of two coincident hits. We write $V_{\text{eff}}^{kk'}(E)$ for a detection of order k in one sensor and of order k' at the NN.

The effective volume depends only slightly on the incoming neutrino direction ϑ , due to the proximity of the average neutrino energy with the energy at which the anisotropy in the positron emission (transition between backward and forward scattering) from the IBD interaction vanishes. Note however that selecting events in the high energy tail of the neutrino emission, where forward scattering is favored, may grant access to the direction of a nearby supernova. This can be done to some extent by means of the coincident hit time analysis.

The current supernova detection strategy with IceCube relies only on $V_{\text{eff}}^1(E)$. We analyze here the power of the new strategy by relying more generally on $V_{\text{eff}}^{kk'}(E)$. We emphasize as well the importance of certain ratios, such as $V_{\text{eff}}^2(E)/V_{\text{eff}}^1(E)$ or $V_{\text{eff}}^{11}(E)/V_{\text{eff}}^1(E)$, which open new perspectives and grant access to new observables, e.g. the average positron energy.

For a given supernova neutrino emission model \mathcal{M} , time-integrated up to time \tilde{t} , the effective volume definition can be extended to embed the spectral shape of the positron energy distribution $d\tilde{\rho}_{e^+}^{\mathcal{M}}/dE$,

$$\tilde{V}_{\text{eff}}^{\mathcal{M}, kk'} = \frac{1}{\tilde{\rho}_{e^+}^{\mathcal{M}}(d)} \int \frac{d\tilde{\rho}_{e^+}^{\mathcal{M}}}{dE}(E, d) V_{\text{eff}}^{kk'}(E) dE, \quad (13)$$

where

$$\tilde{\rho}_{e^+}^{\mathcal{M}}(d) = \int \frac{d\tilde{\rho}_{e^+}^{\mathcal{M}}}{dE}(E, d) dE \quad (14)$$

and which follows from the definition

$$\tilde{N}^{\mathcal{M}, kk'}(d) = \tilde{\rho}_{e^+}^{\mathcal{M}}(d) \tilde{V}_{\text{eff}}^{\mathcal{M}, kk'}. \quad (15)$$

From now on, we drop the \mathcal{M} or replace it by one of the specific models. The presence of the tilde denoting time-integration necessarily refers to a model and confusion in the notation is avoided.

The differential positron density $d\rho_{e^+}/dE_e$ is extracted from the incoming neutrino flux $d\Phi_\nu/dE_\nu$ by folding it

with the differential IBD cross section $d\sigma/dE_{e^+}$ given by Eq. (10) in [38] (accurate up to NNLO in ϵ),

$$\frac{d\tilde{\rho}_{e^+}}{dE_e}(E_e, d) = \rho_p \int \frac{d\sigma}{dE_e}(E_\nu, E_e) \frac{d\tilde{\Phi}_{\bar{\nu}_e}}{dE_\nu}(E_\nu, d) dE_\nu \quad (16)$$

and the total number density of positron interactions (same luminosity for all three models),

$$\tilde{\rho}_{e^+}(10 \text{ kpc}) = \begin{cases} 0.074 \text{ m}^{-3}, & \text{Sf,} \\ 0.096 \text{ m}^{-3}, & T_{\text{FD}} = 5 \text{ MeV,} \\ 0.12 \text{ m}^{-3}, & T_{\text{FD}} = 6.5 \text{ MeV} \end{cases} \quad (17)$$

The proton target density is given by $\rho_p = 2 \rho_{\text{ice}} N_a / M_{\text{ice}}$, where $\rho_{\text{ice}} = 0.91 \text{ g/cm}^3$, $M_{\text{ice}} = 18.015 \text{ g/mol}$, and N_a is the Avogadro constant.

The number of expected events belonging to the various classes $\tilde{N}_{e^+}^{kk'}$ (see Eq. 15), obtained by integration of

$$\frac{d\tilde{N}_{e^+}^{kk'}}{dE_e} = V_{\text{eff}}^{kk'}(E_e) \frac{d\tilde{\rho}_{e^+}}{dE_e}(E_e, d), \quad (18)$$

also defines the relevant observables $\tilde{r}_{kk'}^{jj'} = \tilde{N}_{e^+}^{kk'} / \tilde{N}_{e^+}^{jj'}$, some of them being particularly sensitive to the average energy of the neutrino spectrum.

A. Cherenkov emission

In order to proceed with the effective volume estimates, we need to approximate the average number of detectable Cherenkov photons emitted along the track of a positron with energy E , which could naively be done by combining the Franck-Tamm [39] ($\beta = 1$), the average photomultiplier Q.E. and positron range formulas,

$$N(E) = 2\pi\alpha R(E) \left(1 - \frac{1}{\beta^2 n_{\text{ice}}^2}\right) \int \frac{\chi(\lambda) d\lambda}{\lambda^2} \quad (19)$$

where the integrals for average Q.E and Franck-Tamm formula run between 300 and 650 nm. $R(E)$ is the positron track length above Cherenkov emission threshold and given by [40–42]:

$$R(E) = \ln 2 \ln(1 + E/(E_c \ln 2)) X_0^{\text{water}} / \rho_{\text{ice}}, \quad (20)$$

where $X_0^{\text{water}} = 36.08 \text{ g/cm}^2$, $\rho_{\text{ice}} = 0.92 \text{ g/cm}^2$ and $E_c = 610 \text{ MeV}/(Z + 1.24) = 72.1 \text{ MeV}$ [43].

E.g. at $E = 10 \text{ MeV}$, $R(E) \approx 5.5 \text{ cm}$ and the average number of detectable photons (IC) by a positron is $N \approx 135$. However, Eq. 19 does not take into account Cherenkov photons which are emitted by secondary particles, e.g. knock-off delta electron and positron annihilation. Results from a Geant4 simulation show that the total number of emitted photons remains almost constant (c.f. Fig. 3). In the following we will use the Geant4 photon yield results for the calculations.

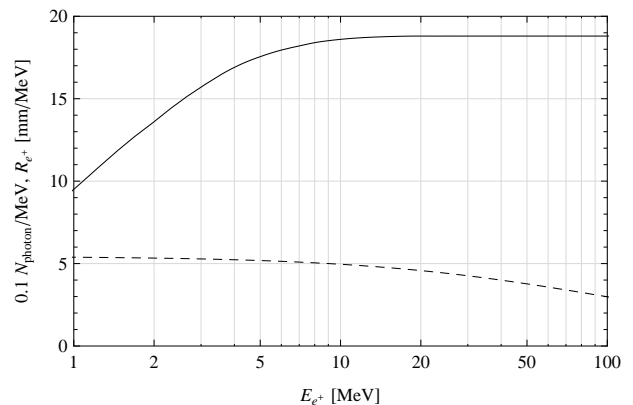


FIG. 3: Number of emitted photon / 10 / MeV by a positron and its byproducts between 300 and 650 nm (Geant4) (solid line) and positron range parametrization above Cherenkov emission threshold in mm/MeV (dashed line) w.r.t. the positron energy.

B. Effective detection volume

The fraction $\epsilon(r, \theta)$ of the 4π sr solid angle occupied by the sensitive surface of the module, viewed under angle θ and at distance r is

$$\epsilon(r, \theta) = \frac{1}{2} \left(1 - \frac{1}{\sqrt{1 + RR(\theta)/r^2}}\right). \quad (21)$$

(we have neglected the spherical shape of the sensor but this remains an excellent approximation).

When $r \gg R$, this expression reduces to

$$\epsilon(r, \theta) = \frac{A_{\text{DOM}}(\theta)}{4\pi r^2}. \quad (22)$$

The expectation number of detected photons is

$$\mu(E, r, \theta) = N(E)\epsilon(r, \theta) \quad (23)$$

We have now all the necessary ingredients to express the coincident hit effective volumes,

$$V_{eff}^k(E_e) = 2\pi \int_R^\infty r^2 dr \int_{-1}^1 d\cos\theta f(k, r, \theta, E_e). \quad (24)$$

$$f(k, r, \theta, E_e) = \frac{1}{4} \left(1 - \sum_{l=0}^{k-1} p_{\mu(r, \theta, E_e)}(l)\right) \quad (25)$$

is the density of probability of recording $\geq k$ hits from a positron with energy E_e , where $p_{\mu(r, \theta, E_e)}(k)$ is a Poisson distribution with mean value

$$\mu(r, \theta, E_e) = 4N(E_e)\epsilon(r, \theta) \exp(-r/\lambda_{\text{abs}}) \quad (26)$$

For the effective volume for a sensor with k hits and NN sensor with k' hits, we can write the more generic expression,

$$V_{eff}^{kk'}(E) = 2\pi \int_R^\infty r^2 dr \int_{-1}^1 d\cos\theta \times 4f(k, r, \theta, E_e)f(k', r', \theta', E_e) \quad (27)$$

where $r' = \sqrt{r^2 + L^2 + 2Lr\cos\theta}$ and $\cos\theta' = (L + r\cos\theta)/r'$.

According to [5] and for the purpose of this estimate, we have made the qualitative assumption that the Cherenkov photons are emitted in correlated directions, roughly over π sr, or a quarter of the sphere, the approximate size of the Cherenkov cone. We therefore effectively implement the anisotropic emission with the inclusion of several factors 4. In order to obtain simple expressions, we have neglected the spacing between the modules which do affect the probability of two NN sensors to be in the pool of photons. This may have a significant impact on the effective volume. We qualitatively argue that most interactions leading to a coincidental hit detection occur slightly below the lower sensor, i.e. θ is in general close to θ' . However, this argument does not hold for 4π sensitive modules. In this case, the expressions derived here are quite approximative.

The correlated probability of photon detection is justified at short distances from the sensor, as the photons are not yet diffused. This correlation gradually vanishes at larger distances and fully disappears at an effective scattering length distance. Fortunately, our assumption is likely quite accurate for NN coincidental hit detection from low energy events, because the detection probability of > 1 photon is sizable only at short distances and the photon directions are not yet decorrelated (i.e. the fraction of contributed events beyond a relatively short distance is negligible, due to a negligible fraction of the subtended areas of the sensors).

The validity of the effective volume formula for single hits with the introduced anisotropic emission holds for arbitrary distance: although large values of the integration variable r (i.e. at distances where the Cherenkov photons and the initial positron directions are decorrelated) contribute significantly to the integral, there is an equivalence at large distances between isotropic emission - uniform low photon expectation value and anisotropic emission - higher photon expectation value within the π sr cone. Stated differently, the equivalence at large distances (i.e. μ small) $f(\mu) \approx 4f(\mu/4)$ (see the expression for $f(\mu)$, Eq. 25).

In Eq. 26, we have introduced a damping factor related to the absorption length. One may question whether we should consider instead the attenuation length as appropriate. This can be understood from first principles (phase space conservation): photons do not propagate to such large distances as they scatter and will only reach an average distance of about an attenuation length from the sensor. However, the subtended sensor area for the photon detection decreases with distance and the large absorption length considered compensates for the shorter

effective distance reached by an average photon but seeing a larger subtended photo-sensor area.

The results for the effective volume in the various detection modes are shown in Fig. 4. It is noticeable that while the ratio of the effective volume to the positron energy for single hit detection mode behaves rather flat and even eventually decreases at high energy, it continually increases for coincidental hit detection modes. The rate of the increase is fastest for the $2+1$ mode and faster for $1+1$ than $2+0$. This behavior reflects in a corresponding increase of the average positron energy for the chosen neutrino emission model. For the four different topologies $1+0$, $2+0$, $1+1$, $2+1$, the relative variation rate with energy is constant, being independent of the specific detector configuration, the absolute scaling of the effective volume, which in turn depends on the quantum efficiency, and the sensor coverage and spacing.

The effective detection volumes in the DDC configuration are significantly higher when the sensor is sensitive over 4π , a factor about three for $1+0$ mode, four for $2+0$ mode and six for $1+1$ and $2+1$ modes around the Garching energy $\langle \tilde{E}_{\bar{\nu}_e} \rangle$.

Fig. 5 shows the detection probability w.r.t. the IBD neutrino interaction location for DC and DDC $_{4\pi}$ configurations.

It is clear from these formulas that, while we constrain ourself to a limited number of detection modes, it is trivial to extend the analysis in order to obtain effective volumes for arbitrary coincidental modes kk' , including those beyond our one dimensional analysis (i.e. modes with hits on different strings which become relevant for a hypothetical configuration with small string spacing).

IV. RESULTS

A. SN detection distance reach

With the effective volumes estimated above, we now have all the ingredients to calculate the number of single and coincidental hit detections. In Table I, we provide the number of detections and the distance reach for unit signal over background information and for a 5σ C.L. detection, calculated for the various configurations with the Sf model, and a comparison of effective volumes in Table II. Note that in the case of the Fermi-Dirac spectrum with $T = 6.5$ MeV and the luminosity L_{BK} calculated by [13], and large area low noise sensors, the $2+1$ detection mode reaches $d_{5\sigma}^{21} = 2.9$ Mpc and $d_{5\sigma}^{11} = 7.2$ Mpc.

The description of the distribution of hit arrival time differences (see [47] and references therein) accounts for the characteristics of the ice, which influences the photon propagation. The shape of this distribution depends on the distance of the sensor from the photon emission location as illustrated in Fig. 6, which shows the arrival time difference of hits at one sensor and its (upper) neighbor (non uniform sensor). We notice that the shape in $2+0$ mode depends weakly on the detector configura-

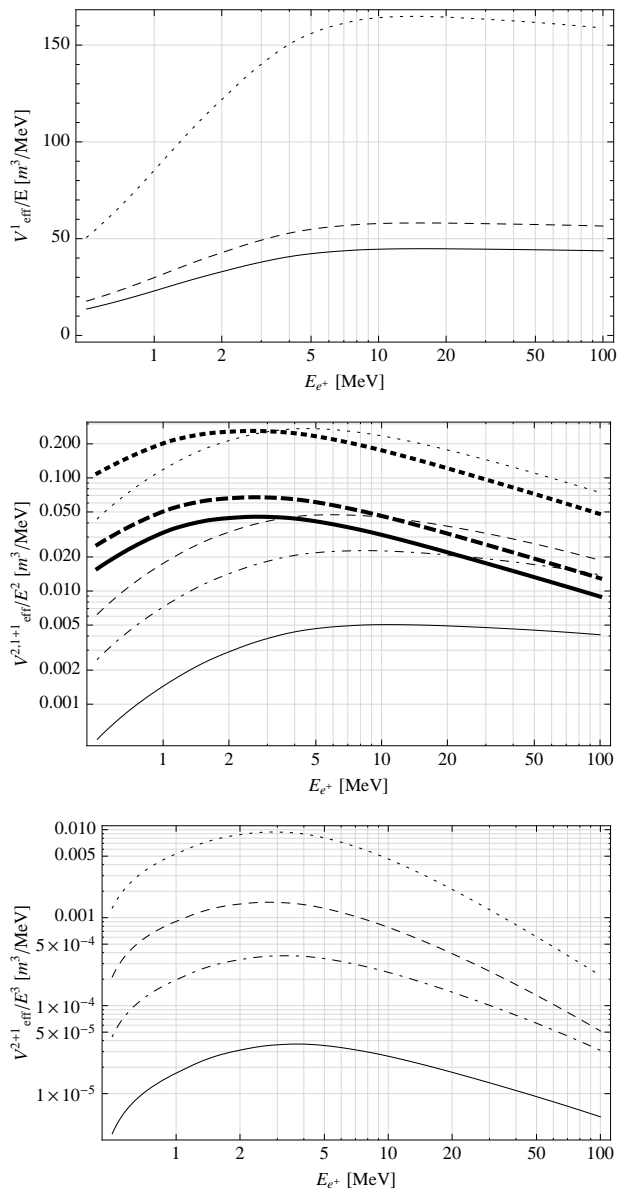


FIG. 4: Upper / middle /lower plots: effective volumes for single hit / coincidental hit / next order coincidental hit. Dotted, dashed, dot-dashed and solid curves resp. for $DDC_{4\pi}$, DDC, DC and IC. Middle plot, thick / thin lines for resp. 2 + 0 and 1 + 1 modes (note that DC and DDC results are the same for 1 + 0 and 2 + 0 modes).

tion, and that a trigger based on the difference of arrival time of hits within $\delta t = 50$ ns catches most of the events ($>95\%$). We use this value for all detector configurations. For the 1 + 1 mode, we optimized the cut on the time difference window $\delta t = t_3 - t_1$ ($t_{1,3}$ are resp. the arrival times at the lower and upper sensor) in terms of $d^{5\sigma}$, and rescaled n_s by the fraction of events surviving the time cuts $\delta t = 50, 100, 150$ ns, resp. for DDC's, DC and IC detector configurations, accordingly.

As we pointed out earlier, the distance reach with

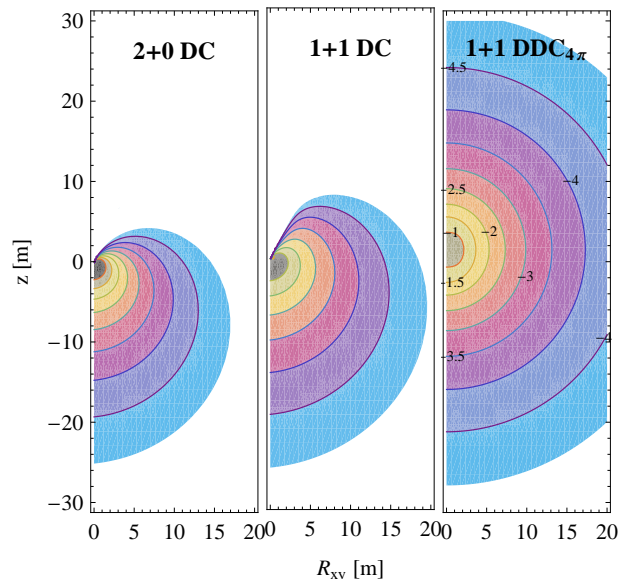


FIG. 5: Detection probability as a function of the interaction for 1+0 and 2+0 modes in DC and 1+1 mode in $DDC_{4\pi}$. The log of the equiprobability contours correspond to the values explicitly shown on the right plot.

$DDC_{4\pi}^{VL}$ and sensor noise reduced to about 100 Hz has a reach larger than 2 Mpc in the 2 + 1 mode, using the benchmark luminosity of [13], twice the IC Q.E., and modules with 50% larger radius. It is eventually limited by the signal statistics and not by the noise, so that it constitutes an upper limit of this > 0.5 Mton (2 + 1 mode) configuration. In order to perform routine SN detection, it is necessary to have $d^{5\sigma} > 4$ Mpc. The detector extension must therefore be significantly more ambitious and provide at least an effective volume of 2 Mton, assuming that the noise is not limiting the reach. For an IceCube extension that would mean the installation of $\gtrsim 10^4$ highly efficient modules, probably with a very small string spacing, in order to collect a substantial amount of events with hits spreading over more than one string. Reducing further the spacing between sensors slightly improves the reach, e.g. to 2.2 Mpc with 2 m, 3 m being quite close to optimal w.r.t. the studied signatures. In conclusion, the realistic implementation of a supernova detector with a reach up to 4 Mpc seems quite demanding from the point of view of costs, deployment time, complexity and R&D, but not unmotivated given the great physics return. Not to mention the improvements it would bring for neutrino studies in the 1 – 100 GeV range (oscillations, indirect search for dark matter, southern sky and low energy neutrino sources).

In conclusion, other projects such as a 0.5 Mton Hyper-Kamiokande [48], or the aforementioned 100 kton LENA [22] would have a quite limited potential as well w.r.t. the detection and characterization of spectral neutrino light curves from extra-galactic supernovae. We therefore confirm that a large multi-Mton effective volume is necessary to this purpose, such as the 5 Mton DEEP

conf.	kk'	$\tilde{V}_{\text{eff}}/m^3$	n_s	n_{bg}	$d^{5\sigma, 1\sigma}/\text{kpc}$
IC	1+0	764	$2.70 \cdot 10^5$	$6.2 \cdot 10^6$	46.5, 104
	2+0	7.4	$2.085 \cdot 10^3$	274	49.9, 108
	1+1	1.7	450	411	20.9, 45.4
	2+1	0.12	26.5	0.02	29.8, 52.0
DC	1+0	990	$2.34 \cdot 10^4$	$4.15 \cdot 10^5$	26.9, 60.1
	2+0	10.8	204	18.3	28.7, 109
	1+1	7.0	122	18.3	22.2, 84.0
	2+1	0.98	13.6	0.001	36.9, 36.9
DDC	1+0	990	$2.62 \cdot 10^5$	$4.67 \cdot 10^6$	49.3, 110
	2+0	10.8	$2.29 \cdot 10^3$	206	55.9, 122
	1+1	12.5	$1.89 \cdot 10^3$	103	59.6, 212
	2+1	2.6	317	0.005	126, 178
DDC $_{4\pi}$	1+0	$2.8 \cdot 10^3$	$7.45 \cdot 10^5$	$4.67 \cdot 10^6$	83.0, 186
	2+0	40.7	$8.64 \cdot 10^3$	206	109, 237
	1+1	58.9	$8.59 \cdot 10^3$	103	127, 452
	2+1	13.9	$1.63 \cdot 10^3$	0.005	285, 403
DDC $_{4\pi}$ 100 Hz	1+0	$2.8 \cdot 10^3$	$7.45 \cdot 10^5$	$1.06 \cdot 10^6$	120, 269
	2+0	40.7	$8.64 \cdot 10^3$	10.6	211, 791
	1+1	58.9	$8.59 \cdot 10^3$	5.31	242, 1116
	2+1	13.9	$1.63 \cdot 10^3$	0.00005	403, 403
DDC $_{4\pi}^{\text{VL}}$ 100 Hz	1+0	$13.0 \cdot 10^3$	$8.0 \cdot 10^6$	$1.06 \cdot 10^6$	394, 880
	2+0	377	$1.86 \cdot 10^5$	10.6	980, 3672
$T_{\text{FD}} = 5 \text{ MeV}$	1+1	582	$1.98 \cdot 10^5$	5.31	1160, 5354
high $L_{\bar{\nu}_e}$	2+1	171	$46.6 \cdot 10^3$	0.00005	2158, 2158

TABLE I: Sensor effective volume for the Garching spectrum, $E_{\text{av}}^+ = 17.1 \text{ MeV}$, various detector configurations and detection modes. The last entries, corresponding to DDC $_{4\pi}^{\text{VL}}$, are results for an enhanced DDC configuration with larger modules and Q.E., for a $T = 5 \text{ MeV}$ Fermi-Dirac spectrum and a luminosity $L_{\bar{\nu}_e}$ normalized to $0.5 \cdot 10^{52} \text{ erg}$.

TITAND [49] project discussed in [13] and designed for routine detection of supernova explosion at a rate of the order 1/yr.

B. Energy spectrum

The hit ratios $(1+1)/(1+0)$ and $(2+0)/(1+0)$ are illustrated in Fig. 7. Both observables are sensitive to the average positron energy and do exhibit a 4.7%/MeV variation around the Garching energy for IC. All configurations exhibit equally strong variations. In addition to their sensitivity to the spectral parameters of the emission spectrum, observables based on ratios have the advantage of canceling some of the involved systematics.

For the benchmark Garching model, Fig. 8 provides the mean values for the neutrino spectrum, the positron spectrum and for IC, for the various coincidental modes. It is noted that the mean energy increases with the mode order.

The resolution on the spectrum will depend on the accumulated statistics and can easily be calculated from the n_s values presented in Table I and the distance. Considering \tilde{r}_{11}^{10} ($N_{10} \gg N_{11}$), the statistical uncertainty is approximately $1/\sqrt{N_{11}}$. Assuming a spectrum obeying Sfl model with a slight uncertainty on $\langle E_{\nu} \rangle$, we can es-

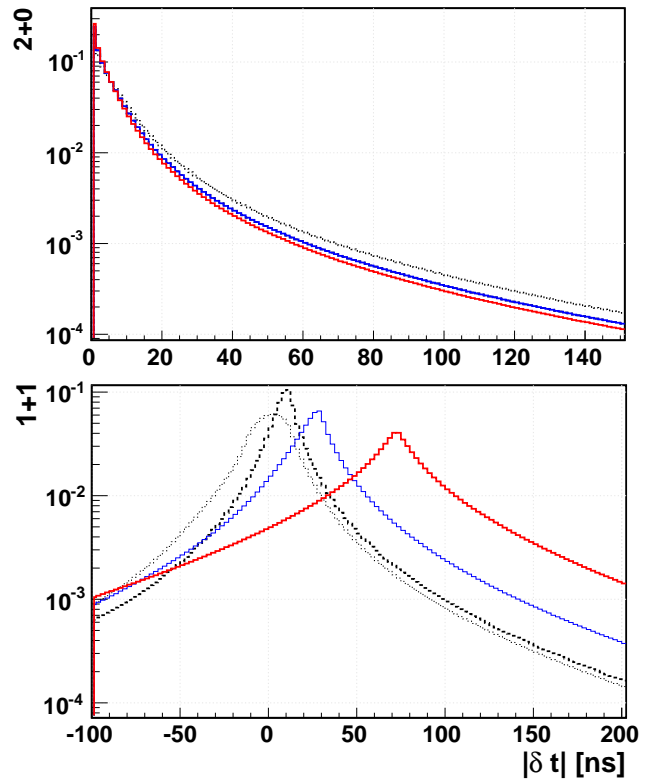


FIG. 6: Difference in hit arrival time. Distributions peaking from left to right correspond to the DDC $_{4\pi}$, DDC, DC and IC configurations.

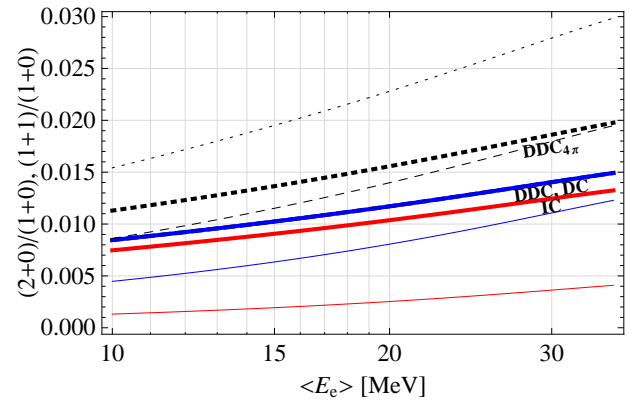


FIG. 7: Coincidental hit ratios $(1+1)/(1+0)$ (thin lines) and $(2+0)/(1+0)$ (thick lines) for DDC $_{4\pi}$, DDC, DC and IC, and w.r.t. $\langle E_{e^+} \rangle$ (the same α was chosen for all $\langle E_{e^+} \rangle$).

timate $\Delta\langle E_{\nu} \rangle$ from the measurements,

$$\Delta\langle E_{\nu} \rangle = \frac{1}{d\tilde{r}_{11}^{10}/dE(\langle E_{\nu} \rangle)\sqrt{N_{11}}}. \quad (28)$$

For example, the statistical error on the fraction $1+1/1+0$ of the signal recorded in the IC configuration

conf.	kk'	$\tilde{V}_{\text{eff}}^{\text{Sf}}$	$\tilde{V}_{\text{eff}}^{\text{FD}, T=5 \text{ MeV}}$	$\tilde{V}_{\text{eff}}^{\text{FD}, T=6.5 \text{ MeV}}$
IC	1+0	764	$1.03 \cdot 10^3$	$1.32 \cdot 10^3$
	2+0	7.4	11.5	16.4
	1+1	1.67	3.00	4.83
	2+1	0.12	0.25	0.45
DC	1+0	990	$1.33 \cdot 10^3$	$1.7 \cdot 10^3$
	2+0	10.8	16.8	24.0
	1+1	7.0	12.2	19.0
	2+1	0.98	1.90	3.20
DDC	1+0	990	$1.33 \cdot 10^3$	$1.7 \cdot 10^3$
	2+0	10.8	16.8	24.0
	1+1	12.5	20.6	30.8
	2+1	2.62	4.62	7.24
DDC $_{4\pi}$	1+0	$2.8 \cdot 10^3$	$3.8 \cdot 10^3$	$4.8 \cdot 10^3$
	2+0	40.7	63.0	90.0
	1+1	58.9	93.2	135
	2+1	13.9	23.4	35.2

TABLE II: Comparison of the sensor effective volume in m^3 for Sf and Fermi-Dirac ($T = 5$ and $T = 6.5 \text{ MeV}$) spectra for the various detector configurations and detection modes.

for a benchmark SN assuming the Sf spectral shape and located at the galactic center is about 5% and does therefore correspond to a resolution on the average energy of about an MeV (and even 0.2 MeV for DDC $_{4\pi}$).

This result is extremely promising and deserves a more sophisticated analysis beyond the scope of this paper in order to study the potential for characterizing the spectral shape of the neutrino flux, and possibly its full evolution, *i.e.* the potential for obtaining the spectral neutrino light curve following a galactic SN.

C. Neutrino flux directionality

In the case of a galactic SN, it is desirable to locate the provenance of the SN neutrinos to inform the community, which could immediately concentrate various instruments toward this target to observe the delayed optical burst. Moreover, it is likely that some supernovae are screened and never detected optically – pointing to the target in advance would result in a large multi-messenger sensitivity gain.

The underlying idea relies on the combination of

1) the fact that the average positron energy leading to coincidental hits is higher than for single hits, as illustrated in Fig. 8, which shows the detected positron spectra for the various modes. There is a gradual increase of the average energy of the modes with an increasing number of hits.

2) an anisotropic scattering of the interaction with a slight preference for photons emitted forward if the higher energy tail of the neutrino emission can be selected. The average interaction $\langle \cos \theta \rangle$ is quite small around SN average neutrino energies. The neutrino interaction is forward scattered above $\approx 14 \text{ MeV}$, which represents between 80 and 90% of the detected neutrinos depending on the coincidental detection mode).

$\langle \cos \theta \rangle = 1\%$ in the 1 + 0 detection mode and rises to approx. 2% in the 1 + 1 detection mode with IC [38] (see the average energies in Fig. 8). In order to exploit this 1% difference, the statistical uncertainty on \tilde{r}_{11}^{10} must be kept smaller and requires therefore large statistics only available below about 2 kpc with IC and 1 kpc with DC (and the azimuth of the incoming direction is not resolved). The situation improves significantly with DDC $_{4\pi}^{\text{VL}}$ which will provide directional information for a SN exploding anywhere in the MW, moreover in a design with small inter-string spacing, the azimuthal direction will be constrained as well (our 1D framework must be extended in order to include inter-string coincidences).

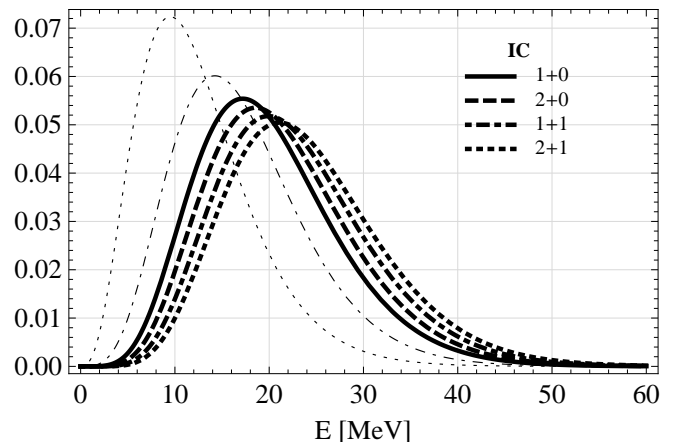


FIG. 8: From left to right. Neutrino (thin, dotted) and positron spectra (Eq. 18): produced (thin, dot-dashed), producing single hit (solid), double hit (dashed), 1 + 1 (dot-dashed) and 2 + 1 (dotted) signatures for IC. The resp. mean energies (in MeV) are:

	ν	e^+	1 + 0	2 + 0	1 + 1	2 + 1
$\langle E \rangle$	12.5	17.1	20.1	21.5	22.85	24.05

It is also clear that the time difference distribution of detected coincidental hits, an observable independent from \tilde{r}_{11}^{10} , should also depend on the angle of provenance of the neutrino flux ϑ .

A careful assessment and quantification of the resolution by studying the impact of the incoming direction on the induced distortion on the hit time difference distribution and the various coincidental hit ratios requires Monte Carlo studies. Such a study should also take into account the elastic scattering channel. Although we pointed out above that the low cross section of this channel will limit its contribution to the overall detection potential, the strong angular correlation and forward peaked cross section might result in a slight enhancement for the measurement of the incidence direction.

V. CONCLUSIONS

In order to confirm the simple analytical calculations for single hit effective detection volume and to precisely

study the new coincident hit detection methodology and the new observables to which it grants access, precise simulation should be performed. In particular, a precise assessment of the angular resolution in locating the SN from the asymmetric Cherenkov emission can be reliably studied as a function of distance and which is only qualitatively stated in this paper.

With such a tool, a dedicated work not focused only on IBD but implementing other neutrino interactions, e.g. with oxygen, would permit the precise assessment of the potential of the novel analysis method for oscillations and matter effect, hierarchy and deleptonization neutrino emission phase studies.

A significant increase in potential would be reached with the imagined $\text{DDC}_{4\pi}^{\text{VL}}$ IceCube extension, with sensors combining several improvements such as a larger and uniform collection surface and an increased photo-detection efficiency (which is of specific interest as the distance reach scales linearly at first order with the Q.E. for 1 + 1 and 2 + 0 detection modes). SN detection up to 2 Mpc would be at hand with the foreseen potential boost of this detector. Such an extension, considerably cost effective compared to similar projects, would be motivated by a broader experimental interest, vastly enhancing the detection potential of low energy neutrinos, $E_\nu \gtrsim 1$ GeV, connected to physics of neutrino oscillations, dark matter neutrino signatures, astrophysical neutrinos in particular from the southern hemisphere, etc [21].

To reach about 2 Mton effective detection volume, thus granting access to SN at distance scales larger of about 4 Mpc and guarantee routine SN detection, the $\text{DDC}_{4\pi}^{\text{VL}}$ configuration is likely too modest and the number of modules should rather be about 10^4 . Also R&D and extensive simulations will be necessary in order to determine the optimal module arrangement, the sensor technology (e.g. the use of solid state detectors instead of PMT, see [51] for a review), and other hardware related parameters.

It is worth mentioning an interesting outcome of this analysis: the method described here can be readily applied to existing and future IceCube data in the regular muon data acquisition mode: events of $\geq 20 \mu\text{s}$ duration are recorded at a rate of about > 2 kHz, *i.e.* representing a lifetime fraction of about 5%, without the necessity of a dedicated data stream. Numbers provided in this paper can readily be rescaled to obtain the reach in the baseline IceCube configuration and its DeepCore provided a corresponding rescaling of the distance reach (by a factor of about 4). Concerning a dedicated data stream, we do not discuss here the possible hardware implications for the realistic implementations of the methodology, but it may well already be implementable within the current IceCube data acquisition hardware.

The methodology is natural for operating [52] and projected [53] water detectors, given a comparatively large noise rate (based on [55], we found in [56] a discussion based on a similar approach).

We finally note that accounting for spin-flavor conver-

sion and MSW effect for neutrinos propagating outward the SN core [54], the $\bar{\nu}_e$ flux is shifted to slightly higher average energy, improving the prospects of the coincidental hit method.

Acknowledgment

We acknowledge fruitful discussions with our colleagues in IceCube, notably L. Köpke. This work is supported by the Swiss National Research Foundation under the grant PP002-114800.

References

- [1] K. Hirata *et al.* [KAMIOKANDE-II Collaboration], Phys. Rev. Lett. **58**, 1490-1493 (1987).
- [2] E. N. Alekseev, L. N. Alekseeva, V. I. Volchenko, I. V. Krivosheina, JETP Lett. **45**, 589-592 (1987).
- [3] R. M. Bionta, G. Blewitt, C. B. Bratton, D. Casper, A. Ciocio, R. Claus, B. Cortez, M. Crouch *et al.*, Phys. Rev. Lett. **58**, 1494 (1987).
- [4] C. Pryor, C. E. Roos, M. S. Webster, Astrophys. J. **329** (1988) 335.
- [5] F. Halzen, J. E. Jacobsen, E. Zas, Phys. Rev. D **53** (1996) 7359.
- [6] L. Hudepohl, B. Müller, H. -T. Janka, A. Marek, G. G. Raffelt, Phys. Rev. Lett. **104**, 251101 (2010).
- [7] H.-Th. Janka, Phys. Rep. **442**, 38 (2007).
- [8] G. G. Raffelt, arXiv:astro-ph/0701677v2.
- [9] A. S. Dighe, arXiv:0809.2977v3 [hep-ph].
- [10] K. Abe *et al.* [T2K Collaboration], arXiv:1106.2822 [hep-ex].
- [11] A. S. Dighe, A. Y. Smirnov, Phys. Rev. **D62**, 033007 (2000).
- [12] S. 'i. Ando, J. F. Beacom, H. Yüksel, Phys. Rev. Lett. **95**, 171101 (2005).
- [13] M. D. Kistler, H. Yüksel, S. 'i. Ando, J. F. Beacom, Y. Suzuki, arXiv:astro-ph/0810.1959.
- [14] M. Ikeda, A. Takeda, Y. Fukuda, M. R. Vagins *et al.*, Astrophys. J. **669** (2007) 519.
- [15] J. Ahrens *et al.* [IceCube Collaboration], Astropart. Phys. **20**, 507 (2004).
- [16] C. Roucelle *et al.* [The IceCube Collaboration], Contr. **1289** to the 31st ICRC, d, Poland (2009).
- [17] Y. Sestayo *et al.* [The IceCube Collaboration], Nucl. Instrum. Meth. **A626-627**, S196-S199 (2011).
- [18] R. Abbasi *et al.* [The IceCube Collaboration], Phys. Rev. **D81**, 057101 (2010).
- [19] C. d. l. Heros, arXiv:1012.0184 [astro-ph.HE].
- [20] R. Abbasi *et al.* [IceCube Collaboration], arXiv:1101.3349 [astro-ph.HE].
- [21] C. Wiebusch *et al.* [IceCube Collaboration], arXiv:0907.2263v1 [astro-ph.IM].
- [22] M. Wurm *et al.* [LENA Collaboration], arXiv:astro-ph/1104.5620.
- [23] A. Rubbia, arXiv:hep-ph/0412230v1.
- [24] S. Choubey, B. Dasgupta, A. Dighe, A. Mirizzi, arXiv:1008.0308v1 [hep-ph].
- [25] P. Antonioli, R. T. Fienberg, F. Fleurot, Y. Fukuda, W. Fulgione, A. Habig, J. Heise, A. B. McDonald *et*

- al.*, New J. Phys. **6**, 114 (2004).
- [26] J. Koskinen *et al.* [IceCube Collaboration], To be published in the Proc. of WIN'11, Cape Town, South Africa (2011).
- [27] P. Kooijman *et al.* [KM3NeT Collaboration], Nucl. Instrum. Meth. **A626-627**, S139-S141 (2011).
- [28] R. Abbasi *et al.* [IceCube Collaboration], Nucl. Instrum. Meth. **A618** (2010) 139-152.
- [29] R. Abbasi *et al.* [IceCube Collaboration], in preparation.
- [30] R. Abbasi *et al.* [IceCube Collaboration], Nucl. Instrum. Meth. **A601**, 294-316 (2009).
- [31] E. Kolbe, K. Langanke, P. Vogel, Phys. Rev. **D66**, 013007 (2002).
- [32] W. J. Marciano, Z. Parsa, J. Phys. G **G29**, 2629-2645 (2003). [hep-ph/0403168].
- [33] http://jp.hamamatsu.com/resources/products/etd/pdf/LARGE_AREA_PMT_TPMH1286E05.pdf
- [34] N. E. Bramall, R. C. Bay, K. Woschnagg, R. A. Rohde, P. B. Price, Geophys. Res. Lett. **32** (2005) L21815 1-4
- [35] M. Honda, T. Kajita, K. Kasahara, S. Midorikawa, T. Sanuki, Phys. Rev. **D75**, 043006 (2007).
- [36] G. D. Barr, T. K. Gaisser, S. Robbins, T. Stanev, Phys. Rev. **D74**, 094009 (2006).
- [37] J. N. Bahcall, A. M. Serenelli, S. Basu, Astrophys. J. **621**, L85-L88 (2005).
- [38] A. Strumia, F. Vissani, Phys. Lett. **B564**, 42-54 (2003).
- [39] I. M. Frank, I. Tamm, C. R. Acad. Sci. URSS **14** (1937) 109-114.
- [40] R. R. Wilson, Phys. Rev. **84**, 100 (1951).
- [41] P. B. Pal, V. P. Varshney and D. K. Gupta, Nucl. Instr. Meth. **B16**, 1 (1986).
- [42] P. B. Pal, S. K. Gupta, V. P. Varshney and D. K. Gupta, Jpn. J. Appl. Phys. **24**, 1070-1073 (1985).
- [43] K. Nakamura *et al.* [Particle Data Group Collaboration], J. Phys. G **G37**, 075021 (2010).
- [44] M. Salathe, master thesis, EPFL, 2011.
- [45] PMT technical paper about afterpulsing
- [46] K. J. Ma, W. G. Kang, J. K. Ahn, S. Choi, Y. Choi, M. J. Hwang, J. S. Jang, E. J. Jeon *et al.*, Nucl. Instrum. Meth. **A629**, 93-100 (2011).
- [47] G. Japaridze and M. Ribordy, arXiv:astro-ph/0506136.
- [48] K. Nakamura, Front. Phys. **35**, 359-363 (2000).
- [49] Y. Suzuki *et al.* [TITAND Working Group Collaboration], arXiv:hep-ex/0110005v1.
- [50] <http://www.ppl.phys.chiba-u.jp/research/IceCube/pmt/GoldenPMT/>
- [51] D. Renker and E. Lorenz, JINST **4** (2009) P04004.
- [52] M. Ageron *et al.* [ANTARES Collaboration], arXiv:astro-ph.IM/1104.1607.
- [53] U. F. Katz [KM3NeT Collaboration], Nucl. Instrum. Meth. **A626-627**, S57-S63 (2011).
- [54] C. Volpe, J. Welzel, arXiv:astro-ph/0711.3237.
- [55] Phys. of Atom. Nucl. **72** (2009) 1537.
- [56] V. Kulikovskiy *et al.*, presented at the XI school "Concentrated energy fluxes in cosmic technics, electronics, ecology and medicine".